Research Article

Instrumentation and High-Speed Photodetector-Based Measurements Reveal Limited Support for the Existence of the Human Aura

Adrian David Cheok[1], **George Karolyi**[2]

1. iUniversity Tokyo, Tokyo, Japan; 2. Mixed Reality Lab, London, United Kingdom

The human aura, a long-debated phenomenon, has been the subject of numerous studies and discussions. This research delves into the potential existence of the aura, examining its characteristics and possible origins. We employ state-of-the-art equipment and methodologies to explore whether the aura is a manifestation of light reflected by skin particles or if the skin itself exhibits a faint self-luminosity, either within or beyond the human-visible light spectrum.

While our investigation provides valuable insights, it is essential to approach the findings with an open mind. The results presented here are based on rigorous scientific methods and should be considered as a significant contribution to the ongoing discourse on the human aura. Our hope is that this research will pave the way for further studies and a deeper understanding of this intriguing phenomenon.

While our study did not provide significant evidence supporting the existence of a human aura, the negative results hold significant scientific importance by offering a critical perspective and contributing to the body of knowledge. Furthermore, our findings can serve as a basis for refuting unfounded claims surrounding the human aura, while also saving engineers valuable time and resources by discouraging redundant projects in the future.

Corresponding authors: Adrian David Cheok, adrian@imagineeringinstitute.org; George Karolyi, george@mixedrealitylab.org

1. Introduction

Throughout history, the notion of an illuminating field encircling the human form, often termed the 'aura', has been a subject of profound intrigue. This luminous entity, frequently illustrated in age-old scriptures and cultural traditions, has been at the heart of both spiritual and academic discourses [1].

In the modern scientific arena, the aura has undergone rigorous examination. The primary aim of such explorations is to identify any physiological or psychological bases that might be associated with its appearance [2]. While some research suggests a potential association between emotional states and aura characteristics, a comprehensive understanding remains to be achieved [3].

The burgeoning domain of biophotonics, which delves into the study of light emissions from biological systems, offers a fresh lens through which the aura can be viewed [4]. Biophotons, or the faint light radiated by living organisms, have been detected in various species, inclusive of humans. It's postulated that these biophotonic emissions might have a direct relation to what has been historically described as the human aura.

Our previous investigations in this field sought to shed light on the potential connection between biophotons and the human aura, employing state-of-the-art imaging techniques and rigorous experimental protocols [2]. While our initial results indicated a possible link, the precise nature and implications of this association warranted deeper exploration.

In this present study, we endeavor to further unravel the complexities of the human aura, probing its potential sources, characteristics, and the myriad factors that might modulate its expression. By amalgamating insights from biophotonics with foundational knowledge from physiology and psychology, we aim to offer a holistic perspective on the aura [5].

Through this scholarly pursuit, our aspiration is to harmonize ancient insights with contemporary scientific understanding, paving the way for a more unified comprehension of the human aura within the broader context of holistic health [4].

While high-speed photodetectors offer promising avenues in the realm of human aura research, they come with their own set of complexities. A predominant concern is the interference caused by noise, which can obscure the accurate detection of the aura. To mitigate this, a spectrum of strategies has been devised. These span from tangible hardware interventions, such as cooling mechanisms for the photodetector to diminish noise, to sophisticated software approaches that employ advanced algorithms for noise filtration from the discerned signal [5].

In the ensuing sections of this manuscript, we delineate an exhaustive exploration centered on the calibration and assessment of high-speed photodetectors tailored for discerning the human aura. Elaborating on the architectural blueprint and operationalization of a counter circuit, we spotlight its efficacy in precisely gauging the photomultiplier anode current pulses within intervals of 10 seconds. Furthermore, we introduce an innovative technique for cooling the photomultiplier, a step that substantially curtails dark counts, thereby enhancing measurement precision. The findings encapsulated herein not only shed light on the nuances of

employing high-speed photodetectors for aura studies but also chart a trajectory for impending explorations in this riveting domain.

2. Literature Review

The notion of a human aura, often visualized as a radiant energy field enveloping the human form, has piqued curiosity across diverse cultural and scientific landscapes [6]. This ethereal phenomenon has garnered renewed attention, especially within the realms of holistic wellness and alternative medicinal practices. This revival is bolstered by technological strides and enhanced instrumentation, facilitating nuanced detection and analysis of the human aura, previously unattainable.

Historical delves into the human aura trace back over a century. A notable figure from this era, physician Walter Kilner, undertook rigorous explorations into the subject during the early 20th century. His insights and observations were meticulously chronicled in his seminal work, "The Human Aura" [7]. What follows is a synthesis of Kilner's pioneering revelations juxtaposed with contemporary assertions on the topic.

While the ability to perceive the human aura remains a rarefied skill, claimed by a select few, some assert that this capability can be honed with dedicated practice. Drawing from accounts of these individuals, we outline a series of recurrent characteristics attributed to the aura in this paper.

The aura doesn't emit its own light and remains invisible in complete darkness. Optimal observation occurs when the individual being observed is positioned approximately 30 centimetres against a dark backdrop, illuminated by soft, scattered light, such as sunlight diffused through curtained windows [8].

The aura seems to be segmented into three distinct layers: the "etheric double", a shadowy gap that spans roughly 0.5 centimetre from the skin; the "inner aura", predominantly blue but can manifest in different hues, stretching 5 to 10 centimetres from the skin; and the "outer aura", a more faintly coloured layer that reaches about 20 centimetres from the skin. On occasion, rays, often emanating from protruding parts like fingers, are observed. A yellowish hue in the aura is often interpreted as a sign of health issues [7].

Observing the aura is more effective on clear days without the presence of mist or haze. Neither temperature nor humidity appears to influence the observation. Enhancing the visibility of the aura can be achieved by illuminating with coloured lights, peering through tinted glass panels, or using dye solutions held between parallel quartz glass containers. Quartz glass is favoured due to its ability to transmit a broader spectrum of light wavelengths. While various tints of blue and carmine proved beneficial, the blue solution of dicyanine dye in alcohol was identified as especially potent [7], [9].

It's posited that one's eyes can be sensitized to discern the aura more effectively by gazing at scattered sunlight through specific dye solutions or tinted glass for a duration. This process seemingly amplifies the unassisted

visual perception of the aura [7].

Although the utilization of coloured illumination or observing the aura via coloured filters can enhance its visibility, it simultaneously modulates the aura's perceived hues. For instance, faintly tinted screens can aid in differentiating between the inner and outer auras, whereas deeper shades primarily reveal the etheric double [7].

The aura's manifestation doesn't seem to be a result of particulates or vapours emanating from the skin, as proximate air currents don't perturb it. There are assertions that subjecting the aura to specific gases or vapours can modify its colour. For instance, chlorine gas exposure renders the aura an orange-green hue, bromine vapours induce a bluish-green shade, while both iodine vapours and ozone gas impart a reddish-brown tint to the aura [7].

Certain individuals might acquire the capability to voluntarily alter their aura's colour or intentionally emit rays. Such intentional hue modifications predominantly impact the inner aura without influencing the outer layer. Hypnosis typically diminishes the aura's magnitude. Additionally, it's posited that electrically charging an individual, especially when they're on an insulated platform, can shrink or even obliterate the aura. Positive charges are more potent in this regard. Upon discharging, the aura re-emerges, potentially exhibiting an augmented size for an extended period [7].

Those professing the skill to perceive the human aura often also assert the capability to discern a mist-like aura around electrically charged conductors and between magnet poles. This could imply an ability to visualize magnetic fields or their atmospheric effects. Moreover, introducing a magnet near a subject reportedly intensifies and merges the auras of both entities, occasionally producing rays between them. Both magnet poles seem equally potent, suggesting the aura's insensitivity to specific poles [7].

The aura's presentation and magnitude seem intrinsically linked to the nervous system's condition. Neurological ailments, cognitive impairments, and episodes of fainting invariably diminish the aura's vibrancy and size. The aura's presence ceases entirely post-mortem [7].

Walter Kilner deduced that after sensitizing his eyes with dicyanine dye screens, he needed to recalibrate his microscope for a clear image. This led him to believe that such sensitization momentarily modified the focal length of his eyes. He inferred from this that sensitization expanded vision towards the ultraviolet spectrum while simultaneously augmenting the capability to discern the human aura. These observations implied that the human aura might encompass light that partially extends into the ultraviolet domain. Furthermore, it suggested that individuals who could perceive the aura might have vision that reaches into the ultraviolet, surpassing the typical visual range of most individuals.

The advancement of high-speed photodetectors has been a pivotal technology enabling progress in aura visualization [10]. Photodetectors are instruments that transform light into electrical impulses. High-speed photodetectors, as implied by their name, can execute this transformation swiftly, making them apt for recording swift alterations in light intensity. Within the realm of human aura research, these apparatuses have been employed to identify and scrutinize the minute fluctuations in the energy aura surrounding humans.

High-speed photodetectors, especially those functioning at rapid velocities, have been utilized extensively across diverse scientific sectors. For instance, in physics, they are employed in light detection experiments, such as those exploring quantum events. In biomedical imaging, photodetectors are integral to technologies like positron emission tomography (PET) and single-photon emission computed tomography (SPECT), which depend on light detection to generate intricate bodily images [11].

Nevertheless, the application of high-speed photodetectors in human aura research presents certain hurdles. A primary obstacle is the intrusion of noise, which can disrupt the human aura's detection. To counteract this problem, an array of strategies has been devised, from hardware-based solutions like photodetector cooling to diminish noise, to software-based approaches like sophisticated signal processing techniques to eliminate noise from the perceived signal [12].

In the current manuscript, we delineate an exhaustive investigation into the calibration and quantification of high-speed photodetectors for the detection of the human aura. We expound on the architecture and realization of a counter circuit tailored to precisely gauge the photomultiplier anode current surges within intervals of 10 seconds. Additionally, we introduce an innovative technique to cool the photomultiplier, which curtails dark counts and augments the precision of our assessments. Our findings offer significant perspectives on the employment of high-speed photodetectors in human aura research, setting the stage for ensuing studies in this intriguing domain [13].

3. Materials and Methods

Over several years, the author, along with his colleagues, embarked on thorough research into the human aura. The central objectives of these studies were to determine whether the aura might be attributed to light reflecting off particles released from the skin or if the skin itself manifested a subtle luminosity, either within or potentially outside the typical visible light spectrum for humans.

Referring to Figure 1, the primary tools employed in these studies were a "monochromator" and a "photomultiplier" photon counting assembly, both housed within a specially designed darkroom. Additionally, essential control and monitoring apparatus were incorporated, details of which will be elaborated upon in subsequent sections. The darkroom was meticulously crafted as a double-walled metallic enclosure, ensuring

minimal light intrusion and offering electrical isolation. The inclusion of dense foam within the double walls further bolstered its resistance to both light and auditory disturbances.

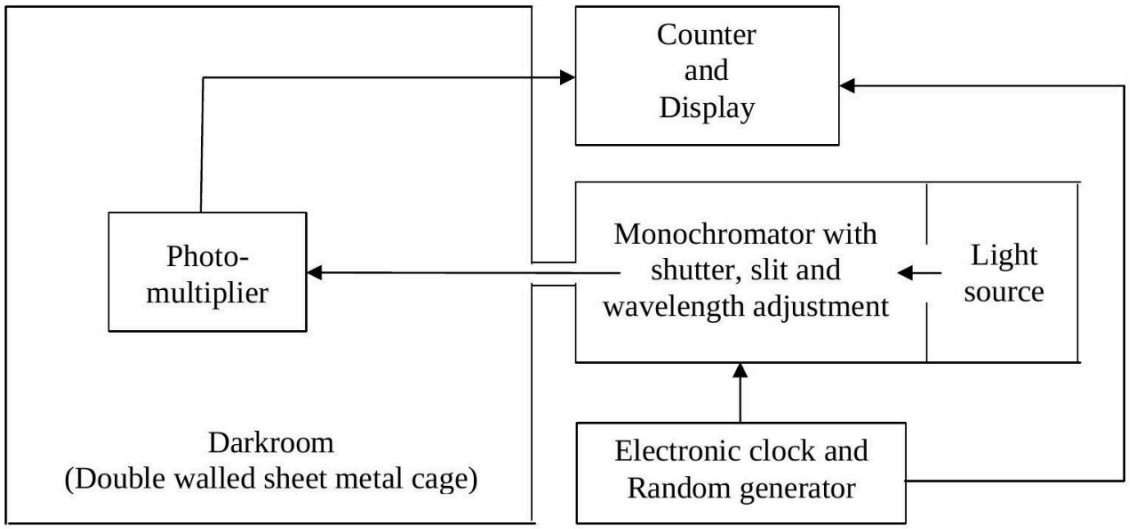

Figure 1. "Monochromator", and a "photomultiplier" photon counting assembly" situated inside a darkroom, together with essential control and monitoring equipment

Typically, light comprises a myriad of electromagnetic waves, each with distinct wavelengths. The purpose of monochromators is to isolate light of a singular wavelength from a source emitting multiple wavelengths. However, due to inherent constraints, the light emitted by monochromators usually spans a tight range of wavelengths, sufficiently close to be deemed, for all practical intents, monochromatic. Monochromators function based on the principles underlying the spectroscope [14]. Within a monochromator, light emanating from a broad-spectrum source is channeled into a slender, flat beam, which is then directed onto one facet of a quartz prism. This light traverses the prism and emerges from its opposite side. The choice of quartz is pivotal, given its capacity to transmit a broader spectrum of light compared to conventional glass. As light rays penetrate and exit the prism surfaces, they undergo refraction, with different wavelengths refracting to varying degrees. Consequently, the emergent light forms a spectrum, segregating light rays based on their respective wavelengths.

The monochromator's design allows for the mechanical rotation of its prism. This rotation adjusts the position of the rays that exit from the prism relative to a slender slit in a stationary opaque plate positioned in the rays' trajectory. By this mechanism, rays of a specific wavelength can be directed to fall on the "output slit" of the stationary plate, passing through it, while rays of differing wavelengths are obstructed by the opaque plate. The rays that emerge from this output slit are nearly monochromatic, essentially having a singular wavelength.

The monochromator depicted in Figure 1 offers the flexibility to select any wavelength ranging from 200 to 2000 nanometres. The typical human observer discerns light within the 400 to 700 nanometre wavelength spectrum, with perceived colors transitioning from violet to red as the wavelength increases within this range. This spectrum is thus termed the visible range, while the regions below 400 nanometres and above 700 nanometres are designated as ultraviolet and infrared, respectively.

The monochromator's output light can be concentrated into a slender beam, which, at a 2-metre distance from the output slit, typically measures 0.5 centimetre in width and 3 centimetres in height. Nearer to the output slit, the beam's cross-sectional dimensions reduce proportionally.

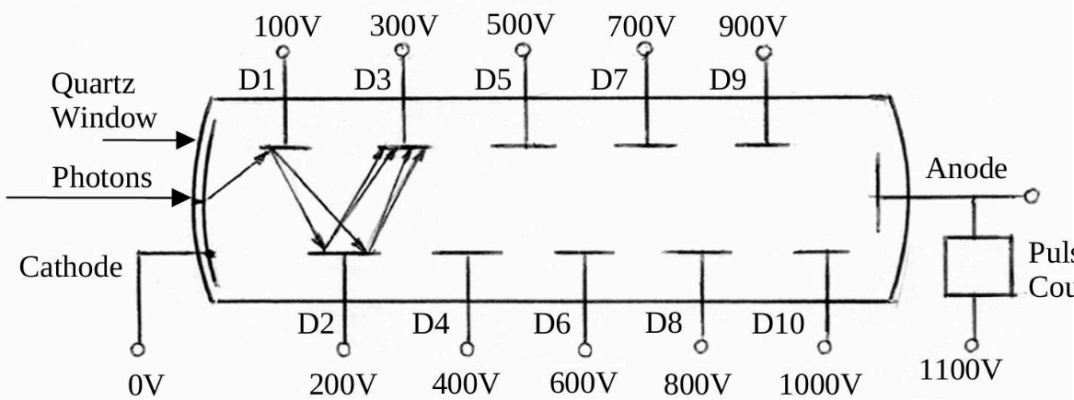

Figure 2. Photomultiplier photon counting assembly

A pivotal feature of the monochromator is its capability to modulate the output beam's intensity, meaning the photon count traversing any segment of the beam every second. This modulation, including dimming the intensity to nil, is achieved by adjusting the width of the output slit. Generally, the emitted light will always span a narrow yet defined wavelength range, contingent on the output slit's width. For instance, with a 0.02 millimetre slit width, the wavelength range might be approximately 1 nanometre. Therefore, if set for an output wavelength of 500 nanometres, the emitted light would peak at this value but also include minor amounts from roughly 499.5 to 500.5 nanometres. Such a monochromator would be attributed with a 1 nanometre resolution. Narrowing the slit width typically results in a more confined output beam and a reduced light wavelength range, indicating enhanced resolution.

The investigations also heavily relied on a photomultiplier photon counting assembly. Central to this assembly is the photomultiplier tube, an evacuated glass enclosure housing multiple electrodes, encompassing a cathode, an anode, and potentially over ten intermediate electrodes termed dynodes. A representation of such a tube, equipped with 10 dynodes, is illustrated in Figure 2.

In one potential configuration, the cathode might be linked to the negative end of a 1100-volt direct voltage source. Concurrently, the anode would connect to the positive terminal of this source via an electronic current pulse counter mechanism. This voltage source would have taps at approximately 100-volt intervals, enabling the dynodes to be connected sequentially, ensuring each subsequent dynode is 100 volts more positive than its predecessor. Hence, dynodes D1, D2, D3,... D10 would be 100, 200, 300,... 1000 volts more positive than the cathode, and the anode would be 1100 volts more positive in relation to the cathode. This arrangement establishes electric fields between the cathode, the dynodes in sequence, and the anode. Typically, the cathode is designed as a semi-transparent electron-emitting layer on the interior of a quartz window.

Imagine a photon striking and traversing the quartz window, reaching the semi-transparent electron-emitting cathode layer. A photon with adequate energy might induce the cathode to release an electron. This electron, propelled by the electric field between the cathode and dynode D1, gains kinetic energy. Upon reaching dynode D1, it might trigger the release of multiple electrons. These electrons, in turn, are driven to dynode D2 by the electric field between D1 and D2. As they strike D2, each electron might release several more electrons. This cascading effect amplifies the electron count at each stage. If an electron's impact on a dynode results in the release of four electrons, then the final count of electrons reaching the anode could exceed a million for each initial electron from the cathode. This surge of electrons at the anode forms a discernible electric current pulse, which can be tallied by the electronic current pulse counter circuit.

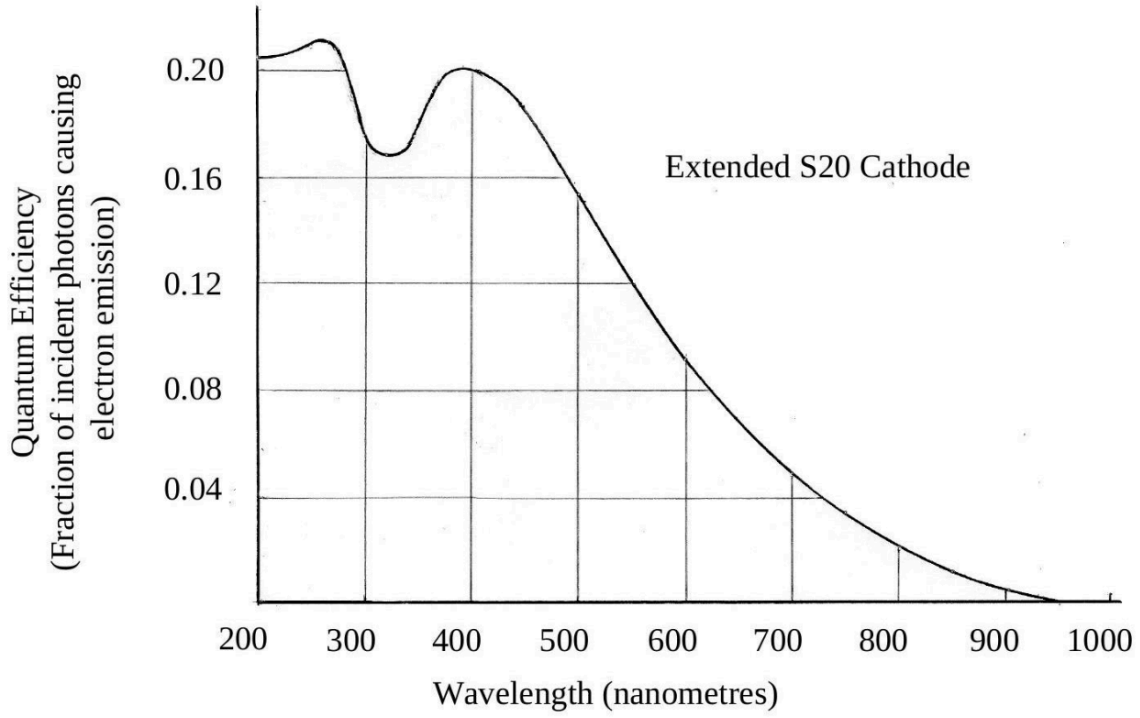

Figure 3. Quantum efficiency

The cathode's sensitivity to photons, given its ability to emit electrons when struck by photons, earns it the moniker "photocathode". However, not every photon impacting the cathode leads to electron emission. Therefore, the count over a specific duration represents only those photons that, upon reaching the cathode, possess enough energy to induce electron emission. Photons with insufficient energy to trigger this emission are not included in the count.

As a result, the electron count from the cathode during any time frame is always a subset of the total photons hitting the cathode. This ratio is termed the "quantum efficiency", and it varies based on the photon's wavelength, the window's material, and the chemical makeup of the electron-emitting cathode layer. Practical experiments can determine the quantum efficiency. Figure 3 illustrates the relationship between quantum efficiency and photon wavelength for the specific photomultiplier used in the described research.

The monochromator's graph, as depicted in Figure 3, spans from 200 to 950 nanometres in wavelength. The curve's termination at 950 nanometres is attributed to the specific photomultiplier's cathode coating used in our research, which remained unresponsive to wavelengths beyond 950 nanometres in the infrared spectrum. Conversely, in the ultraviolet domain, the coating was responsive to wavelengths considerably below 200 nanometres. However, the quartz window's photon transmissibility diminishes drastically below 200

nanometres. As a result, the functional wavelength range of the tube was confined between 200 and 950 nanometres.

It's noteworthy that the actual photon count can be inferred from the electron count, provided the quantum efficiency is known. Although the term "electron count" is precise, it's colloquially referred to as the "photon count", and the apparatus is often dubbed a photon counter.

A point of clarification: the photocathode, being a semi-transparent layer on the photomultiplier's inner window surface, essentially shares the same effective area as the window. Additionally, a minor fraction of photons impinging on the photomultiplier window get absorbed by the window and never reach the photocathode. This negligible effect is accounted for in the quantum efficiency curve shown in Figure 3. Henceforth, terms like "photomultiplier window", "photocathode", or simply "window" or "cathode" are used synonymously.

In the research delineated here, it was paramount to ensure that only photons from the designated source, be it a human subject or a monochromator, reached the photocathode, while all extraneous light was rigorously excluded. To achieve this, the photomultiplier photon counter assembly was ensconced in a meticulously constructed darkroom. The monochromator's output light beam was channeled into this darkroom through a lightproof conduit, ensuring it impinged on the photomultiplier window perpendicularly, maintaining a typical distance of 2 metres from the beam's entry point.

The cathode's circular area, with a diameter of 4.5 centimetres, was aptly sized to accommodate the incoming light beam. One of the photomultiplier's less desirable traits is its propensity to generate "dark" current pulses, leading to corresponding dark counts, even in the absence of incident light. These pulses arise from the atomic thermal vibrations within the cathode's electron-emitting coating.

To mitigate the dark counts and the potential errors they introduce, the photomultiplier was encased in a cooling apparatus, allowing the photocathode's temperature to be lowered to approximately -30^{O} Celsius. This temperature reduction curtailed atomic vibrations and the resultant electron emissions to a level that yielded an acceptable dark count rate for our research objectives.

For the entirety of the research detailed in this paper, the electronic current pulse counter circuit was meticulously designed to enumerate the photomultiplier anode current pulses within precisely measured 10-second intervals, as dictated by an electronic timing mechanism.

There were two primary counting methodologies employed. The first, termed the "single count method", necessitated manual initiation via a push button. Subsequent to the initiation, the circuit would tally the number of anode current pulses over the ensuing 10 seconds.

The second approach, dubbed the "continuous count method", was more automated, with the electronic clock producing periodic auditory signals to demarcate successive 10-second intervals. To provide a tangible example, consider a scenario where the monochromator's output light wavelength is calibrated to 500 nanometres, and the output slit is adjusted such that the net count (with the shutter open) exceeds the dark count (with the shutter closed) by 200 counts per second.

Referring to Figure 3, the number of photons impinging on the cathode each second would be:

$$\begin{aligned}&(\text{number of photons falling on the cathode per second})\\&= \frac{\text{number of electrons emitted per second}}{\text{quantum efficiency at 500 nanometres}}\\&= \frac{200}{0.153} \approx 1310\end{aligned} \tag{1}$$

The energy of each 500 nanometre photon is:

$$\begin{aligned}&(\text{Planck's constant}) \times (\text{photon frequency})\\&= (\text{Planck's constant}) \times (\text{speed of light}) / (\text{photon wavelength})\\&= \frac{\left(6.625 \times 10^{-34} \text{ joule second}\right) \times \left(3 \times 10^{8} \text{ metres per second}\right)}{\left(500 \times 10^{-9} \backslash \text{ metre}\right)}\\&= 3.975 \times 10^{-19} \text{ joule}\end{aligned}$$

The energy delivered to the cathode by the number of photons falling on the cathode per second, in joules per second, is then:

$$\begin{aligned}&(\text{energy per photon in joules})\\&\times (\text{number of photons delivered per second})\\&= \left(3.975 \times 10^{-19}\right) \times (1310)\\&\approx 5.21 \times 10^{-16} \text{ joule per second}\\&\approx 5.21 \times 10^{-16} \text{ watt.}\end{aligned}$$

It's essential to understand that the term "power" refers to the energy generated, conveyed, or utilized every second. Measured in watts, one could equivalently state that the power the photons impart to the cathode upon impact is 5.21×10^{-16} watt.

To elucidate the methodology employed in examining the auras of individual participants, often termed "subjects", let's delve into the specifics. As previously mentioned, the monochromator's emitted light beam was directed into a sealed metal enclosure, targeting the photomultiplier window roughly 2 metres from where the beam entered. En route to the window, the beam was designed to traverse between two aligned, horizontal protrusions. Within the enclosure, the subject was strategically positioned so that various body parts, including the head, hand, arm, and torso, lightly touched the protrusions' edges. This arrangement ensured the light beam flowed parallel to the subject's skin surface, maintaining a predetermined gap. By adjusting the protrusions in relation to the beam, this gap could be modified, ranging from 0.5 centimetres up to 15 centimetres.

4. Results

It's anticipated that if the aura is composed of particles emanating from the skin, then some photons traveling near the subject's body might be reflected back towards their source or at least deflected, preventing them from reaching the photocathode. This implies that aura observers are witnessing light reflected from aura particles, similar to how one sees an object by perceiving light reflected from it.

The aura's reflective properties might vary across wavelengths. Additionally, if the light beam's intensity is too high, the photon density near the skin might overshadow the number of skin-emitted particles, making any reflection or deflection negligible. The beam's proximity to the skin could also play a role.

To address these variables, tests were conducted across various beam intensities, wavelengths, and distances from the skin using six subjects. Despite the limited number of subjects, the depth and duration of each test provided significant insights. No count reduction was observed, suggesting that the monochromator light beam travels near the human body without interference. This indicates that the aura doesn't reflect light from any substances emitted from the skin within the 200 to 950 nanometre wavelength range.

Further tests were conducted with the photomultiplier positioned near the light beam's entry point into the cage. The objective was to detect any scattered light. Again, no scattered light was detected, reinforcing the conclusion that the aura doesn't reflect or scatter light within the tested wavelength range.

The next question was whether the aura might have a faint self-luminosity. Tests were conducted using non-reflecting rectangular horns mounted in front of the photomultiplier housing window. Yet again, the results were negative, indicating no detectable self-luminosity in the tested wavelength range.

The focus then shifted to the skin's surface. While the skin reflects incident photons, it was questioned if it exhibits detectable self-luminosity. Tests were conducted using a collimator tube mounted in front of the photomultiplier housing window. The results indicated photon emission from all tested body parts, with fingertips being the most prominent emitters.

Initial tests focused on three fingertips. Counts were taken over successive 10-second periods with and without the fingers in place. The results, shown in Figure 4, identified subjects by their initials to maintain confidentiality.

Figure 4 reveals that subject G.K. had the highest initial net count, which decayed over time. In contrast, subject P.B.'s count fluctuated with minimal decay, while subject A.D.'s count was intermediate. The dark count, taken without fingers, remained relatively stable.

The results in Figure 4 are comprehensive, encompassing photons of any wavelength within the photomultiplier's range. This raised questions about the number of photons emitted within specific wavelength

subranges and their associated energies, leading to inquiries about energy distribution across wavelengths.

A method to gather such data involves placing optical filters between the fingertips and the photomultiplier housing's window. A "band-pass" filter is designed to permit photons within a specific wavelength range to traverse it while obstructing photons outside this range. The transmission curve of a band-pass filter, as depicted in Figure 5, illustrates the proportion of incident photons that the filter allows to pass through at distinct wavelengths during a set time frame.

From the graph, it's evident that as the photon wavelength increases, the transition from blocking to allowing passage and then back to blocking is not abrupt, and a full 100% transmission is never achieved. The filter's transmission curve can be determined by obtaining net counts from a monochromator at various wavelengths, placing the filter in front of the photomultiplier housing's window, and then comparing it without the filter. The net counts are the difference between the counts from the monochromator and the dark counts.

For the current investigations, it's feasible to approximate the filter curve with a rectangular shape, as illustrated by the dashed lines in Figure 5. This rectangle has the same peak as the filter curve, and its boundaries are defined such that areas A and B are equal, and areas C and D are also equal. This provides a standardized pass range for the filter, represented by the rectangle's base, which spans from wavelength λ_1 to λ_2. Within this range, the photon transmission fraction is assumed to be constant and equivalent to the rectangle's height. It's important to note that, given the area equivalences mentioned, the total area beneath the actual filter curve matches the rectangle's area.

By placing the filter in front of the photomultiplier housing's window (and thus, in front of the photocathode), one can obtain "active" counts from the fingertips. "Dark" counts can also be recorded without the fingertips over alternating 10-second intervals. The mean of the differences between consecutive active and dark counts provides the average net count. From this, one can deduce the average energy reaching the photocathode over a 10-second span from three fingertips situated 17 centimetres away from the cathode, within the λ_1 to λ_2 wavelength range.

In real-world applications, more accurate results can be achieved using "long-pass" filters. These filters block photons with shorter wavelengths and allow those with longer wavelengths to pass. The transition from blocking to allowing passage becomes more gradual as the photon wavelength increases. Figure 6 displays the transmission curves of two such long-pass filters, labeled F_1 and F_2. These curves represent the fraction of incident photons that a filter allows to pass through at various relevant wavelengths within a specific time frame.

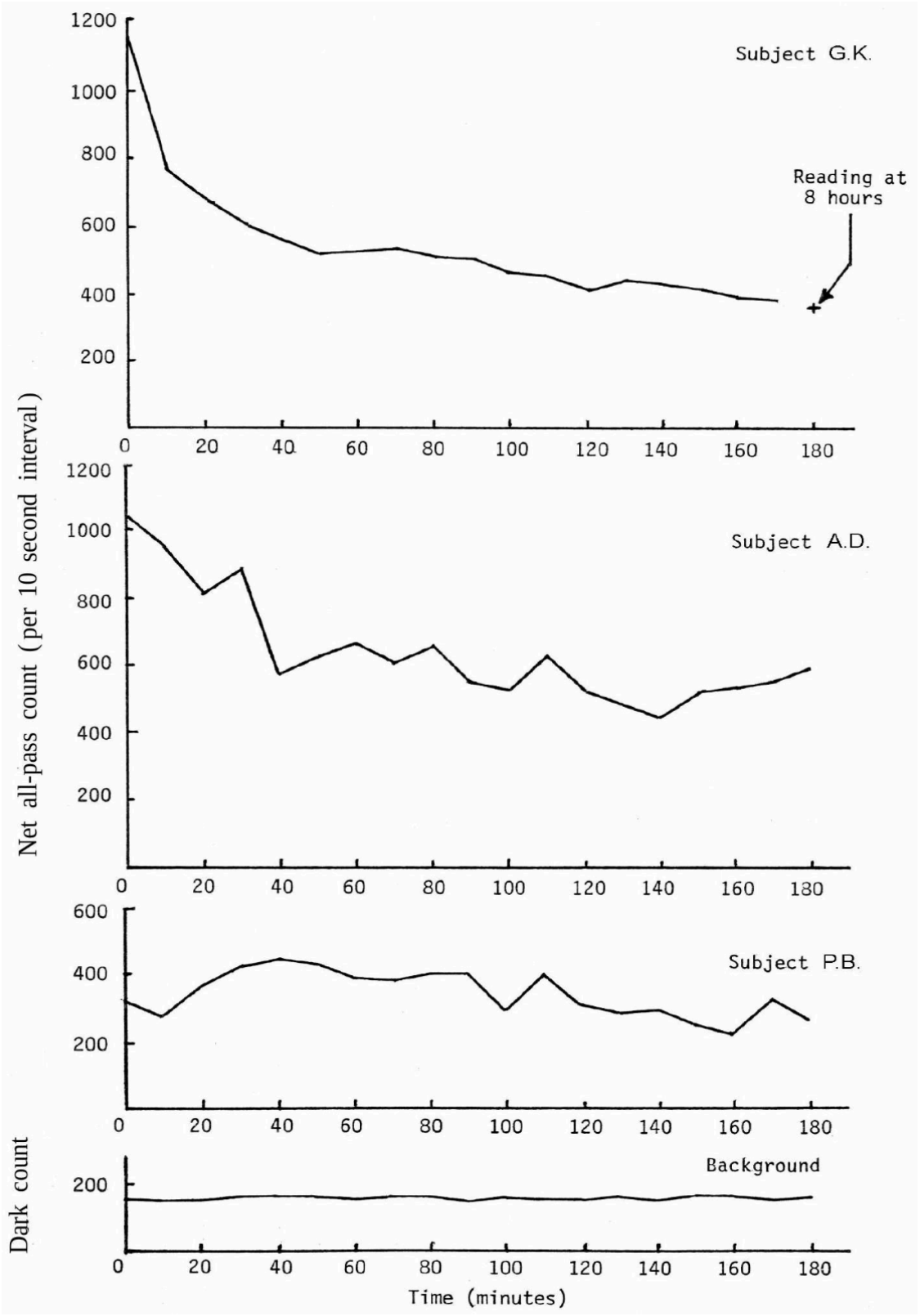

Figure 4. Selfluminosity experimental study

doi.org/10.32388/EB41QY

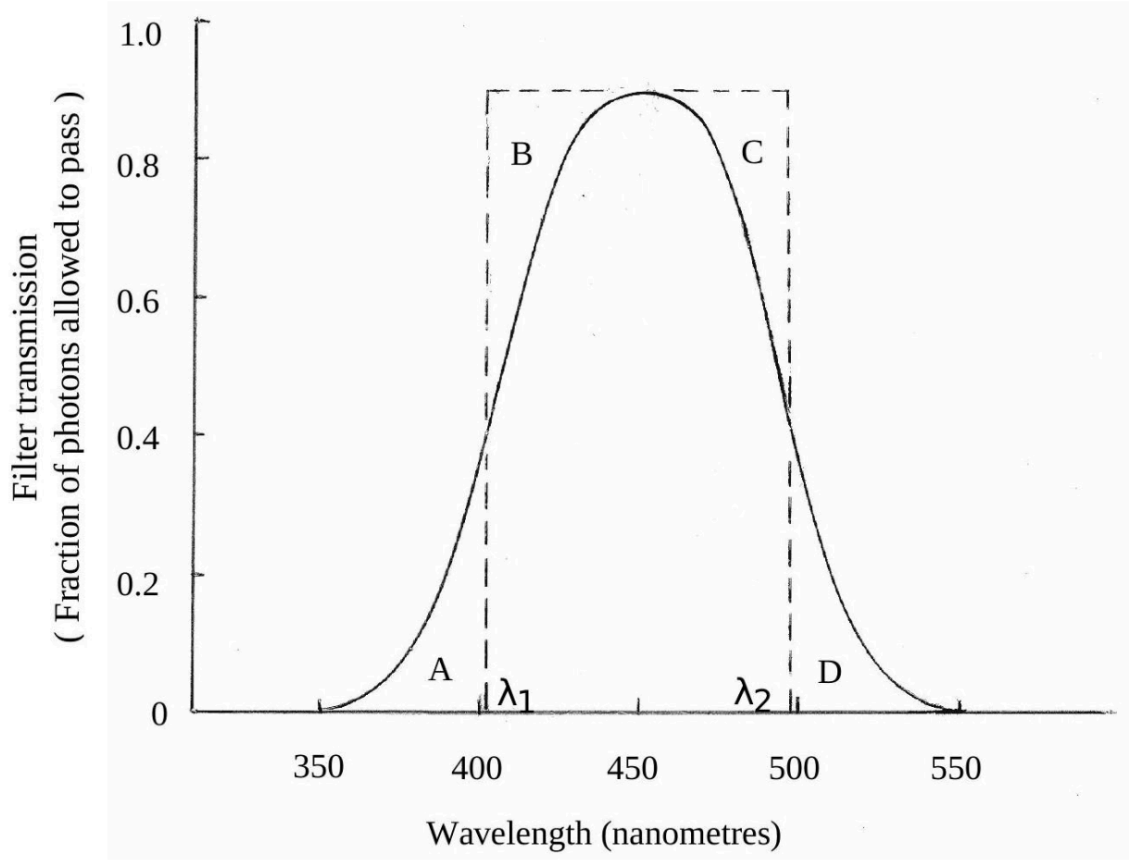

Figure 5. Band-pass filter transmission curve

doi.org/10.32388/EB41QY

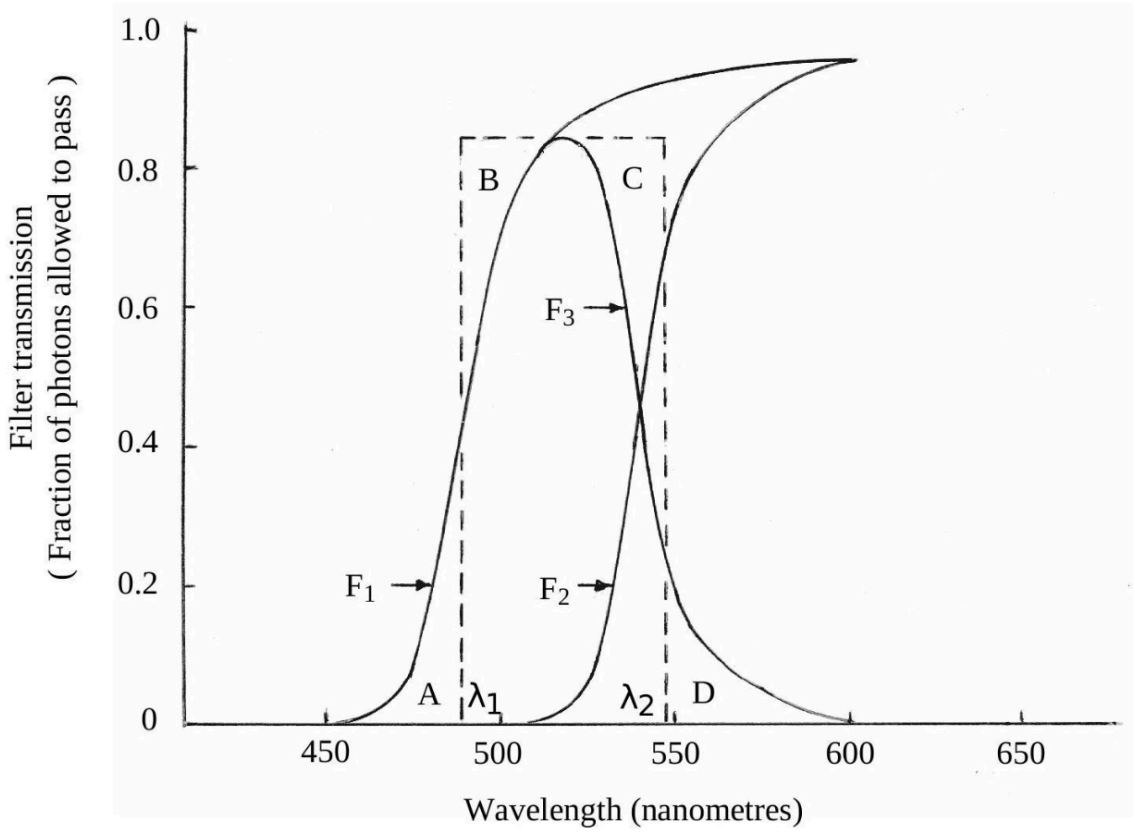

Figure 6. Two long pass filter results

When one captures active counts from the fingertips using two consecutive long-pass filters over two 10-second intervals and then takes their difference, the outcome mirrors what would be achieved using a single corresponding band-pass filter. The filter curve for this equivalent band-pass filter, represented as F_3 in Figure 6, is derived by subtracting the two long-pass filter curves on a wavelength-by-wavelength basis. By employing the rectangular approximation of the filter curve F_3 (shown as dashed lines in Figure 6), one can achieve the same results as with a single band-pass filter. The rectangle's height matches the peak of the filter curve F_3, and its base, $(\lambda_2 - \lambda_1)$, is determined similarly to the method used in Figure 5. Within the wavelength range λ_1 to λ_2, the fraction of photons transmitted by this idealized filter equals the rectangle's height. Outside this range, all photons are blocked. Utilizing long-pass filters offers two primary benefits: the elimination of the need for dark counts and the ability to achieve narrower wavelength ranges.

The average net count is derived from the mean of several differences between active counts captured using two long-pass filters over successive 10-second intervals. From this average, one can determine the average energy reaching the photocathode within the λ_1 to λ_2 range, just as with band-pass filters.

doi.org/10.32388/EB41QY

By combining both band-pass and long-pass filters, the photomultiplier tube's entire wavelength range (200 to 950 nanometres) was segmented into nine distinct subranges. Notably, there are minor overlaps and gaps between these subranges due to filter availability constraints. To facilitate filter changes, the filters were mounted on a rotatable wheel, enabling swift and efficient filter swaps.

It's essential to remember that at any given wavelength, only a subset of photons striking the photomultiplier window induces electron emission from the cathode. This fraction fluctuates across wavelengths, as depicted in Figure 3. If the wavelength range λ_1 to λ_2 is sufficiently narrow, one can assume a near-constant fraction within this range.

While counts were typically recorded over 10-second intervals for practicality, the energy reaching the photocathode within a specific wavelength range is usually calculated on a per-second basis. This involves working with the average net count per second, which is the 10-second average net count divided by 10.

The energy that actually reaches the photocathode per second through the idealized filters in Figures 5 and 6 is reduced since these filters don't transmit all photons within their respective λ_1 to λ_2 ranges. The energy of interest is the amount emitted from the fingers that would reach the photocathode per second, 17 centimetres from the fingertips, within an ideal filter's λ_1 to λ_2 range. Calculating this energy value from the average net count per second involves several steps:

(energy that would reach the photocathode per second within the λ_1 to λ_2 range at 100% transmission

$$\frac{\left(\begin{array}{c}\text{energy per photon at the}\\ \text{middle of the } \lambda_1 \text{ to } \lambda_2 \text{ range}\\ \text{in joules}\end{array}\right)\times\left(\begin{array}{c}\text{number of photons which actually}\\ \text{reaches the cathode per second within}\\ \text{the } \lambda_1 \text{ to } \lambda_2 \text{ range through the filter}\end{array}\right)}{\left(\begin{array}{c}\text{fraction of photons passing the filter in the } \lambda_1 \text{ to } \lambda_2 \text{ range}\\ = \text{ height of the rectangle in Figure 4 or 5}\end{array}\right)}$$

where one has: (energy per photon at the middle of the λ_1 to λ_2 range in joules)

$$= \frac{\left(\begin{array}{c}\text{Planck's constant}\\ 6.625\times10^{-34}\text{ joule second}\end{array}\right)\times\left(\begin{array}{c}\text{speed of light}\\ 3\times10^{8}\text{ metres per second}\end{array}\right)}{(\text{ wavelength at the middle of the } \lambda_1 \text{ to } \lambda_2 \text{ range in metres })}$$

and also:

$$\left(\begin{array}{c}\text{number of photons which actually reaches the cathode}\\ \text{per second within } \lambda_1 \text{ to } \lambda_2 \text{ range through the filter}\end{array}\right)$$

$$= \frac{(\text{ net count per second within the } \lambda_1 \text{ to } \lambda_2 \text{ range })}{\left(\begin{array}{c}\text{fraction of the incident photons on the photomultiplier window}\\ \text{resulting in electron emission from the photocathode at the centre of the}\\ \lambda_1 \text{ to } \lambda_2 \text{ range}\end{array}\right)}$$

For instance, two specific long-pass filters employed in the conducted tests were Wratten 29 and Wratten 92. Utilizing the filter curves of these filters, as depicted in Figure 6, the height of the idealized rectangle was determined to be 0.96. The base, $(\lambda_2 - \lambda_1)$, spanned from 660 to 612 nanometres, resulting in a width of 48

nanometres and a central wavelength of 636 nanometres. Referring to Figure 3, at 636 nanometres, the proportion of photons impinging on the photomultiplier window that lead to electron emission from the photocathode is 0.073 (equivalent to 7.3%). The mean of 50 net counts using the aforementioned filters was 370 over a span of 10 seconds, translating to 37 counts every second. This leads to the following calculation:

(number of photons arriving at the photocathode each second)

$= (37)/(0.073) \approx 507$ photons per second,

(energy per photon at 636 nanometre)

$= \left(6.625 \times 10^{-34}\right) \times \left(3 \times 10^{8}\right) / \left(636 \times 10^{-9}\right) \approx 3.13 \times 10^{-19}$ joule,

and so:

$$\begin{pmatrix} \text{energy reaching the photocathode per second within the} \\ \text{612 to 660 nanometre wavelength range at 100\% filter transmission} \end{pmatrix}$$

$$\begin{aligned} & \left(3.13 \times 10^{-19}\right) \times (507)/(0.96) \\ = & \approx 1.65 \times 10^{-16} \text{ joule per second} \\ & \approx 1.65 \times 10^{-16} \text{ watt.} \end{aligned}$$

In the subsequent discussions, the term "energy reaching the photocathode per second through a filter" will refer to the energy per second at a full 100% filter transmission, within the filter's pass range from λ_1 to λ_2.

We define "power density" as the power (or energy per unit time) arriving at the photocathode for each nanometre of wavelength. This is calculated by dividing the energy per second within the λ_1 to λ_2 wavelength interval by the width of that interval, i.e., $(\lambda_2 - \lambda_1)$. For the aforementioned scenario, the calculation is:

(power density) = $\left(1.65 \times 10^{-16}\right) /(660 - 612) \approx 3.44 \times 10^{-18}$ watt per nanometre.

Following this methodology, one can ascertain both the power (energy every second) and the power density (energy for each nanometre) that reaches the photocathode from three fingertips situated 17 centimetres away from the photocathode, within the specified wavelength intervals. The outcomes of this analysis are illustrated in Figure 7, showcasing the results for the same trio of subjects whose cumulative net count was previously evaluated within the photomultiplier's 200 to 950 nanometre wavelength spectrum.

and depicted in Figure 4. Each bar in Figure 7 represents the mean of 50 measurements, derived from five separate tests, conducted on distinct days spaced at least a week apart, with each test contributing 10 readings per bar. It was mentioned earlier that minor overlaps and gaps existed between the idealized filter wavelength intervals. In Figure 7, the boundaries of these intervals have been slightly adjusted, positioning them at the midpoints of the overlaps and gaps, thus simplifying their elimination. (Due to these minor modifications, the 612 to 660 nanometre interval mentioned earlier becomes 613 to 661 nanometres, which has an inconsequential impact on the derived outcomes).

As illustrated in Figure 4, subject G.K. displayed a significant decrease in the all-pass count over time. Therefore, for G.K., during each test, two sets of 10 net count readings per bar were recorded: one immediately upon entering the cage and another an hour later. In Figure 7, these are represented by the top of each bar and the horizontal line within each bar, respectively. The difference between these two readings indicates the reduction in power density over an hour. Specifically, the aforementioned calculation for the 612 to 660 nanometre range, resulting in a power density of 3.44×10^{-18} watt per nanometre, corresponds to the readings for G.K. immediately after entering the cage, as can be verified from Figure 7.

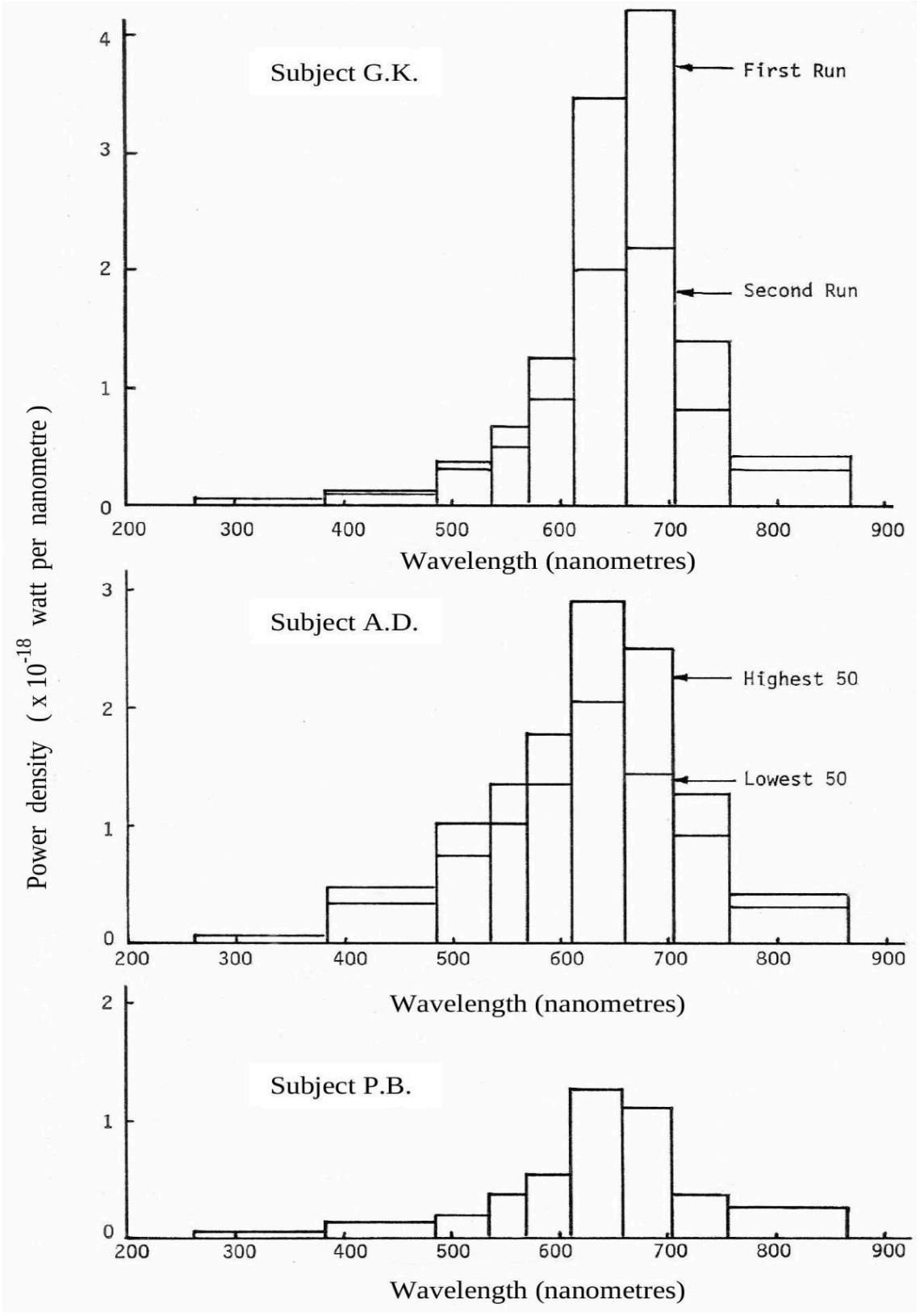

Figure 7. Power density

doi.org/10.32388/EB41QY

For subject A.D., who displayed minor decay but more pronounced fluctuations in the all-pass count (as seen in Figure 4), Figure 7 presents two sets of results. These are based on the average of the 50 highest and 50 lowest readings, represented by the top of each bar and the horizontal line within, respectively.

For subject P.B., who showed minimal decay and slight fluctuations in the all-pass count in Figure 4, only a single set of results is presented in Figure 7.

In Figure 7, the area of each rectangle, calculated as the product of its base and height, represents the power that would be received by the photocathode from three fingers through the corresponding ideal filter. This assumes that the filter would allow all photons within its designated wavelength range and block those outside. The cumulative power received by the photocathode, under these assumptions, is the sum of the areas of all the rectangles in Figure 7.

Thus, in 7, for G.K. immediately after entering the cage, considering the adjusted filter wavelength ranges that eliminate gaps and overlaps, the combined area of the rectangles can be approximated as:

$$\begin{aligned}
&(870-759)\times\left(0.5\times10^{-18}\right)+(759-706)\times\left(1.3\times10^{-18}\right)+(706-661)\times\left(4.3\times10^{-18}\right)\\
&+(661-613)\times\left(3.4\times10^{-18}\right)+(613-573)\times\left(1.1\times10^{-18}\right)+(573-536)\times\left(0.7\times10^{-18}\right)\\
&+(536-487)\times\left(0.3\times10^{-18}\right)+(487-383)\times\left(0.1\times10^{-18}\right)+(383-263)\times\left(0.05\times10^{-18}\right) \qquad (2)\\
=&(55.5+68.9+193.5+163.2+44.0+25.9+14.7+10.4+6.0)\times10^{-18}\\
=&582\times10^{-18}=5.82\times10^{-16}\ \text{watt}.
\end{aligned}$$

This represents the energy associated with the photons that can potentially reach the photocathode. However, the total number of photons emitted from the three fingertips significantly surpasses the number that can actually reach the photocathode. Assuming that the photons emitted from the fingers disperse uniformly in all directions, and only those on a direct path from the fingertips to the photocathode reach it (disregarding any photons that might reach the cathode via reflections from nearby structures, like the inner surface of the collimator tube), the following relationship can be established:

$$\begin{aligned}
&\frac{(\text{total number of photons emitted from the fingers per second})}{(\text{number of photons reaching the cathode per second})}\\
&=\frac{(\text{surface area of a sphere with a 17 centimetre radius})}{(\text{surface area of the cathode with a 2.25 centimetre radius})}\\
&=\frac{4\times\pi\times17^2}{\pi\times2.25^2}\approx\frac{3630}{15.9}\approx228
\end{aligned}$$

Here, we've used the approximation $\pi \approx 3.14$ for the calculations related to circular and spherical areas.

While the assumptions made might introduce some errors, the derived value should be viewed as a maximum estimate. Nevertheless, it's reasonable to believe that the total number of photons emitted from the fingers every second could be about 100 times (or more) than the number reaching the photocathode every second. This implies that the overall power radiated from the three fingers is on the order of 10^{-14} watt.

A key observation from the spectral distributions in Figure 7 is that, despite the extremely low power levels, the majority of the photon emission is in the visible spectrum, predominantly within the 600 to 700 nanometre range, which corresponds to visible red light. The ability of observers to perceive light emissions at these minimal power levels will be discussed later.

Photon emissions from other body parts, aside from the fingers, were too minimal to determine spectral distributions using optical filters. However, general all-pass counts were achievable as previously described in relation to Figure 4. These counts were obtained using the previously mentioned 5 centimetre diameter collimator tube, ensuring that only photons originating from a 5 centimetre diameter area of the body's surface could contribute to the count.

Average net counts were derived from seven distinct body surface areas, focusing on the palm, nose, forehead, right eye, left eye, chest, and abdomen, for the same three subjects whose results are depicted in Figures 4 and 7. The experimental approach involved recording active counts over 10-second intervals for each body surface area, followed by 10-second dark counts with the body surfaces removed. The difference between active and dark counts provided the net counts. This method was repeated 10 times in a session, yielding 10 net counts for each body area. The duration of these sessions varied up to an hour, depending on unavoidable pauses between consecutive 10-second counting intervals and any breaks requested by the participants.

Five such sessions were conducted on separate days, typically spaced a week apart, for each participant, resulting in a total of 50 net counts for each body area per participant.

	Subject G.K.			Subject A.D.			Subject P.B.		
Part of Body	Count per second	Photons per second	Power $\times 10^{-16}$ watt	Count per second	Photons per second	Power $\times 10^{-16}$ watt	Count per second	Photons per second	Power $\times 10^{-16}$ watt
Fingers	128	1910	5.8	126	1880	5.7	51	760	2.3
Palm	46	690	2.1	64	960	2.9	53	790	2.4
Nose	20	280	0.91	37	550	1.7	24	360	1.1
Forehead	14	210	0.63	26	390	1.2	12	180	0.54
Right Eye	18	250	0.82	21	310	0.95	15	220	0.68
Left Eye	16	240	0.72	17	240	0.77	16	220	0.72
Chest	7.9	120	0.36	6.8	100	0.31	4.0	60	0.18
Abdomen	5.1	76	0.23	2.9	43	0.13	6.0	90	0.27

Table 1. Power from various parts of the body

The average net count per second is simply the 10-second average net count divided by 10. These per-second averages can be translated into energy emission estimates (or power) by assuming that photon emissions from all body areas are primarily in the 600 to 700 nanometre wavelength range, as observed for the fingers. Hence, it's plausible to assume that all photon energies correspond to the midpoint of this range, i.e., 650 nanometres. Additionally, the fraction of photons impacting the photomultiplier window that induce electron emission from

the photocathode is the value corresponding to a 650 nanometre wavelength in Figure 3, which is 0.067. This leads to:

(energy per photon at 650 nanometres in joules)

$$= \frac{\left(\begin{array}{c}\text{Planck's constant}\\ 6.625 \times 10^{-34}\text{ joule second}\end{array}\right) \times \left(\begin{array}{c}\text{speed of light}\\ 3 \times 10^{8}\text{ metres per second}\end{array}\right)}{\left(\text{wavelength } 650 \times 10^{-9}\text{ metre}\right)}$$

Hence, (energy reaching the photocathode per second in watts)
$= \frac{(\text{energy per photon at 650 nanostructures in joules}) \times (\text{average net all pass count per second})}{(\text{fraction of photons falling on the cathode causing electron emission at 650 nanometers})}$
$\approx \left(3.06 \times 10^{-19}\right) \times (\text{average net all pass count per second})$
$/0.067 \approx (\text{average net all pass count per second}) \times \left(4.56 \times 10^{-18}\right)$ watt.

Therefore, by dividing the average net count per second by 0.067, we can determine the number of photons that reach the photocathode every second. Furthermore, by multiplying the average net count per second by 4.56×10^{-18}, we can ascertain the average power (in watts) that reaches the photocathode through the collimator tube from the specified 5 centimetre diameter body surface areas. The results derived using this method are presented, rounded to two significant figures, in Table 1. It's worth noting that the results for the fingertips were determined using a more precise approach, which involved summing the areas of the rectangles in Figure 7.

The collimator tube was treated with an anti-reflective material. Given that once photons are emitted, they can disperse in every conceivable direction from the body's surface, the majority would come into contact with the non-reflective interior of the collimator and be absorbed. Only a minor portion would navigate to the cathode due to internal reflections of the collimator. Drawing parallels to the previous discussion about fingers, the photon emission from body regions with a 5 centimetre diameter might be nearly 100 times the figures presented in Table 1. A review of Table 1 reveals that subsequent to the fingers, the palm and nose are primary photon emitters, whereas the chest and abdomen areas emit less. Notably, G.K., who exhibited the most significant photon emission, did not assert any supernatural capabilities, whereas A.D. and P.B., with diminished photon emission, professed psychic capabilities, including healing talents. The data in Table 1 doesn't indicate a correlation between photon emission and professed psychic talents.

In the historical context of this chapter, Walter Kilner, a prior researcher, hypothesized that the aura might be linked to light emission beyond the visible spectrum, and those who perceive it might have vision that transcends the typical visible spectrum. Yet, Figure 7 suggests that photon emission from human fingertips is minimal in the ultraviolet and infrared spectrum, making it an improbable source of the aura some individuals perceive.

Subsequent tests were conducted to compare the 'bandwidth of vision' across various subjects, essentially the spectrum within which different individuals can perceive light. Among the subjects tested were individuals who professed the ability to perceive the human aura and those who didn't.

Key equipment for these tests included the previously described lightproof cage situated in a room devoid of windows, a monochromator in the neighboring lab, with its light output channeled into the cage via a lightproof connector, and a photomultiplier photon counting mechanism inside the cage. The light beam from the monochromator was directed perpendicularly onto the window of the photon counting mechanism inside the cage, positioned roughly 2 metres from the light entry point. Test subjects were positioned such that their heads were slightly below the photomultiplier's window. A concave lens made of quartz was positioned at the cage's light entry to expand the light beam's cross-sectional area. This ensured that both the photocathode and the subject's eyes experienced the same light intensity. The lens was quartz to ensure ultraviolet light transmission.

The monochromator could adjust the light's wavelength from 200 nanometres in the ultraviolet spectrum to 2000 nanometres in the infrared. Its output slit's width was modifiable, allowing for the adjustment of light intensity. As previously noted, the monochromator's light output typically encompasses a range of wavelengths, but this can be confined to half a nanometre on either side of the desired value by minimizing the slit width.

To ascertain if a subject can perceive light of a specific wavelength and intensity, a mere affirmative or negative from the subject isn't sufficient. A statistical methodology is imperative. Subjects would intermittently hear beeps from an electronic timer via an intercom. Between beeps, the monochromator's light would either enter the cage or be obstructed by a light trap controlled by a random electronic generator linked to the timer. Subjects had access to two buttons, labeled 'yes' and 'no'. The 'yes' button was to be pressed if light was detected, and 'no' if it wasn't. For each wavelength and intensity setting, subjects were prompted for 30 consecutive button presses. Responses could be a mix of 'yes' and 'no', and their accuracy would align with Table 2.

When specific wavelength and intensity values resulted in a subject providing 30 accurate "yes" responses, it was deduced that the subject could clearly discern the light. Conversely, if out of 30 responses, approximately half were accurate and the other half were not, it was inferred that the subject was merely speculating, leading to the conclusion of their inability to detect the light. The likelihood of such outcomes being purely coincidental or speculative will be elaborated upon in Chapter 6. For now, it's pertinent to note that the odds of achieving 20 or more accurate responses from 30 trials due to mere speculation is below 5%. At this probability threshold, it's generally accepted that 20 or more accurate responses from 30 trials indicate genuine light perception,

albeit potentially challenging. In contrast, 19 or fewer accurate responses would signify the subject's inability to discern the light.

Light on or off	Button Pressed	Response
On	Yes	Correct
Off	No	Correct
On	No	Incorrect
Off	Yes	Incorrect

Table 2. Push button logic

To encompass the monochromator's entire wavelength spectrum, two distinct light sources were deemed essential. An incandescent lamp with a tungsten filament catered to the spectrum's longer wavelengths, inclusive of infrared, while a mercury vapour lamp was utilized for shorter wavelengths, inclusive of ultraviolet. The tungsten lamp emits a continuous spectrum, allowing for any wavelength to be selected for testing. Conversely, the mercury lamp emits a discontinuous spectrum with a limited number of distinct spectral lines, restricting tests to these specific wavelengths.

It was observed that a subject's vision bandwidth was influenced by light intensity. Hence, the decision was made to operate at the lowest light intensity that was discernible by all test subjects within the 400 to 700 nanometre wavelength range, typically deemed visible to humans. Utilizing the tungsten lamp and setting the monochromator's output light to 650 nanometres, the intensity was incrementally augmented until all eight subjects consistently provided 30 accurate responses.

Consequently, at 650 nanometres, every subject consistently responded accurately 30 times at an approximate electron count of 30,000 per second. With these settings, each subject underwent further testing. The wavelength was augmented in increments of 25 nanometres, and the accurate responses were recorded for each increment. The maximum wavelength that still resulted in 20 or more accurate responses was deemed the subject's vision limit at the spectrum's infrared end.

For assessing the vision limit at the ultraviolet spectrum end, the tungsten lamp was substituted with the mercury vapour lamp. Six prominent spectral lines from this lamp were selected for testing, rounded to the nearest nanometre as $436, 405, 365, 334, 297$, and 254 nanometres. Due to rounding discrepancies and the inherent inaccuracy of wavelength dials, minor adjustments were essential after setting the monochromator to any of the aforementioned values to maximize the electron count per second.

Psychic Subjects		Control Subjects	
G.B.	405 – 700	G.K.	405 – 700
M.B.	405 – 725	D.N.	365 – 700
P.B.	365 – 700	H.W.	365 – 725
M.S.	365 – 850	J.M.	297 – 700

Table 3. Bandwidth of vision tests

Similar to the infrared spectrum tests, at 436 nanometres, every subject consistently responded accurately 30 times at an electron count of 3,000 per second, which is a tenth of the count at 650 nanometres. This discrepancy can be attributed to the heightened photon energies, quantum efficiency, and ocular sensitivity at diminished wavelengths. The testing procedure entailed setting the slit to yield an electron count of 3,000 per second at the 436 nanometre spectral line, followed by recording each subject's accurate responses for the aforementioned spectral lines in descending wavelength order. The minimum wavelength still resulting in 20 or more accurate responses determined the subject's vision limit at the ultraviolet spectrum end.

Of the eight subjects tested, half professed psychic capabilities, inclusive of perceiving the human aura, while the remainder did not, serving as control subjects. The vision bandwidth test outcomes for these subjects are tabulated in Table 3, detailing each subject's vision limits in nanometres.

Upon examining the data in Table 3, it becomes evident that the vision bandwidth for the initial three psychic participants, as well as the first trio of control subjects, aligns closely with the universally recognized visible spectrum ranging from 400 to 700 nanometres. Intriguingly, psychic participant M.S., boasting a vision spectrum from 365 to 850 nanometres, exhibited enhanced perception into the infrared domain but lacked ultraviolet vision. Conversely, control participant J.M., with a vision range from 297 to 700 nanometres, demonstrated heightened ultraviolet perception but no infrared vision. Given M.S.'s results, one might speculate a potential association between the human aura and the infrared spectrum. However, the pronounced aura-seeing claims by psychic G.B. compared to the more tentative assertions by M.S. challenge this hypothesis. The overarching inference suggests that while certain individuals exhibit vision beyond the standard visible spectrum, those professing aura-seeing capabilities don't necessarily possess a broader vision bandwidth. Consequently, the phenomenon of aura perception doesn't seem to be attributed to extended vision into the ultraviolet or infrared domains.

A subsequent query emerged regarding the potential of psychics, who assert their capability to perceive the human aura, to discern light emissions from human skin, as delineated in Table 4.1. Given that psychic G.B. in Table 3 was the most assertive in claiming aura perception, it was deemed pertinent to determine this subject's

"vision threshold". This refers to the minimal photon quantity traversing a 1 square centimetre area perpendicularly, per second, which G.B. could consistently discern at the wavelengths 436 and 650 nanometres.

The testing methodology mirrored the one employed for ascertaining subjects' vision bandwidth. However, modifications were made to gradually diminish the monochromator output slit at the wavelengths 436 and 650 nanometres until the participant barely achieved 20 accurate responses from 30 trials, signifying the vision threshold's attainment. This procedure was reiterated multiple times. The mean of the discrepancies between electron counts during active light and blocked light conditions at the vision threshold provided the "net vision threshold electron count per second" for psychic G.B. at the aforementioned wavelengths. Derived from these, several pertinent metrics, elaborated in the subsequent section, are tabulated in Table 4, with all values approximated to two significant figures.

Wavelength in nanometres	436	650
Net threshold of vision electron count per second	250	3000
Quantum efficiency	0.19	0.067
Number of photons striking the cathode per second	1300	45,000
Cathode area in square centimetres	16	16
Number of photons striking the cathode per square centimetre per second	83	2800
Energy per photon in joules	4.6×10^{-19}	3.1×10^{-19}
Light intensity reaching the cathode and the eyes in watts per square centimetre, at the threshold of vision	38×10^{-18}	870×10^{-18}
Light intensity reaching the cathode from three fingers, 17 centimetres from the cathode, in watts per square centimetre	2.0×10^{-18}	35×10^{-18}
(Intensity at threshold) / (Intensity from fingers)	19	25

Table 4. Net threshold of vision electron count per second

In Table 4, the net threshold electron count per second, divided by the appropriate quantum efficiency from Figure 3, gave the number photons falling on the photocathode per second. The number of photons striking the cathode per square centimetre per second was obtained as the number of photons falling on the cathode per second, divided by the cathode area in square centimetres. In Table 4, light intensity is understood to be energy

carried by photons across 1 square centimetre area, perpendicular to the motion of the photons, in 1 second, and is measured in units of joules per square centimetre per second. But, since energy created, carried, or expended, per second is called power, light intensity may also be designated as power carried across 1 square centimetre area perpendicular to the motion of the photons, and measured in units of watts per square centimetre. Thus, in Table 4.4, light intensity reaching the photocathode, or the eyes, in watts per square centimetre, at the threshold of vision, was calculated as the number of photons striking the cathode per square centimetre per second, multiplied by the energy of 1 photon in joules at the relevant wavelength. This then gave 38×10^{-18} watt per square centimetre at the 436 nanometre wavelength, and 870×10^{-18} watt per square centimetre at the 650 nanometre wavelength.

These were then compared with the light intensity falling on the cathode from three fingers of subject G.K., 17 centimetres from the cathode, as given in Figure 7. Subject G.K. was chosen as the one with the highest photon emission. Now, unlike the vision tests, the photons reaching the cathode from the fingertips had a continuous wavelength distribution. To allow for this, the overall wavelength range was divided into two parts, namely:

Firstly, the power within the 263 to 536 nanometre wavelength range, which equalled the sum of the first three rectangular areas in Figure 7, and which for subject G.K. added up to 31×10^{-18} watt falling on the window, or upon division by the cathode area, yielded a light intensity of 2.0×10^{-18} watt per square centimetre.

Secondly, the power within the 536 to 870 nanometre wavelength range, which equalled the sum of the last six rectangular areas in Figure 7, and which for subject G.K added up to 551×10^{-18} watt falling on the window, or upon division by the cathode area, yielded a light intensity of 35×10^{-18} watt per square centimetre.

It is seen that the threshold intensity at 436 nanometres was 19 times the intensity falling on the cathode from the fingers within the 263 to 536 nanometre wavelength range, while the threshold intensity at 650 nanometres was 25 times the intensity reaching the cathode from the fingers within 536 to 870 nanometre wavelength range.

It had to be concluded that psychic subject G.B. could not be able to see the light emitted from three fingers at a distance of 17 centimetres, by a large margin. The question then arose, if light intensity arriving at the eyes of an observer from the whole body of a subject, at an increased distance, could be discernible to the observer. Now, light intensity is known to fall off with the square of the distance from the source of the photons. This means that if the fingers were viewed at 1.7 metres, instead of 17 centimetres, that is at 10 times the distance, the observed light intensity would be 1/100 of that seen at 17 centimetres.

Light intensity reaching the eyes of an observer from the whole body of a subject, viewed at some fixed distance, is rather difficult to estimate. A very rough figure could be deduced by estimating the whole skin surface area of the body, and with the aid of the information in Table 1, estimating the total power emitted by

the whole body. Then, remembering that emitted photons travel not only in a direction perpendicular to the skin, but in all directions, and also that light intensity falls with distance, a rough estimate for the light intensity reaching the eyes of an observer, 1.7 metres from the subject, could be arrived at. An approximate calculation along these lines for subject G.K., relying on Table 1, yielded 10^{-17} watt per square centimetre, which has been rounded to the nearest order of magnitude. (Orders of magnitude are: 10^{N} or 10^{-N} where N = any whole number).

It has to be recalled that most photon emission from the skin occurs within the 600 to 700 nanometre wavelength region. Consequently, the above 10^{-17} watt per square centimetre intensity needs to be compared with the threshold of vision intensity at 650 nanometres in Table 4.4, namely 870×10^{-18} watt per square centimetre, or 10^{-15} watt per square centimetre when rounded to the nearest order of magnitude. Thus, it is seen that the above deduced light intensity of 10^{-17} watt per square centimetre is below the threshold of vision, as rounded to 10^{-15} watt per square centimetre, by a factor of 100, or two orders of magnitude. This leads to the conclusion that the observer would not be able to perceive the light emitted from the whole body of a subject at a distance of 1.7 metres.

Let it now be supposed that the observer's eyes are replaced by the photomultiplier, which then has an intensity of 10^{-17} watt per square centimetre falling on its photocathode. Since this intensity is approximately 1/100 of the threshold intensity, the corresponding net electron count per second would also be around 1/100 of the net threshold electron count of 3000 per second at 650 nanometres in Table 4, that is, approximately 30 per second, or 300 over a 10 second period.

It is to be noted that photomultipliers can be expected to yield good results only from small areas of skin, with the aid of collimator tubes excluding stray photons. Nevertheless, tests were carried out with the subjects standing in the cage, 1.7 metres from the photomultiplier at waist height, and no collimator attached. Dark counts, over 10 second periods, were typically around 300, increasing to around 450 with the subjects in front of the tube, yielding net counts around 150 over 10 seconds. The readings were thus greatly affected by background stray photons, partly due to exhaled air by the subjects, which was found to be a substantial source of photon emission, persisting for long periods after a subject has left the cage. Lower than expected counts may also be explained by the fact that many photons emitted by the subject strike the cathode obliquely, and consequently are less effective in producing electron emission. Nevertheless, the predicted and measured net counts were of the same order, they could not be considered contradictory.

It is claimed that the aura is best seen in subdued light, such as may be present in a curtained room. Any such subdued light would exceed the emission from the skin by many orders of magnitude, and completely swamp it, thereby rendering it invisible even if the observer could possibly see light emitted from the skin.

Furthermore, observers of the aura claim to see colours. Now, not only is the light emitted from the skin essentially visible red, but light of any colour seen at low levels of intensity, approaching the threshold of vision, appears greyish to all observers. The eye has the ability to distinguish colours only at much higher levels of intensity.

Thus, all indications are that observers claiming the ability to see the human aura do not perceive physical light, that is photons emitted or reflected. The claimed ability to see auras is akin to the claimed ability to see "ghosts". Such abilities, if real, constitute paranormal phenomena which is not in our realm of electrical engineering.

In Table 4, the net threshold electron count per second, when divided by the corresponding quantum efficiency from Figure 3, yielded the number of photons impinging on the photocathode every second. The photon count per square centimetre per second was derived by dividing the total photon count by the cathode's area in square centimetres. In Table 4, light intensity is defined as the energy conveyed by photons across a 1 square centimetre area, orthogonal to the photon's trajectory, in a span of 1 second. This is quantified in joules per square centimetre per second. However, since energy generated, transported, or expended per second is termed power, light intensity can also be described as power traversing a 1 square centimetre area perpendicular to the photon's motion, quantified in watts per square centimetre. Consequently, in Table 4, the light intensity reaching the photocathode or the eyes, in watts per square centimetre at the vision threshold, was computed by multiplying the photon count per square centimetre per second by the energy of a single photon in joules at the pertinent wavelength. This resulted in values of 38×10^{-18} watt per square centimetre at 436 nanometres and 870×10^{-18} watt per square centimetre at 650 nanometres.

Comparing these values with the light intensity emanating from the fingers of subject G.K., positioned 17 centimetres from the cathode as depicted in Figure 7, revealed interesting insights. G.K. was selected due to the highest photon emission among subjects. Unlike the vision tests, the photons reaching the cathode from the fingertips exhibited a continuous wavelength distribution. To account for this, the entire wavelength range was bifurcated into:

1. The power within the 263 to 536 nanometre wavelength range, equivalent to the sum of the initial three rectangular areas in Figure 7. For subject G.K., this totalled 31×10^{-18} watt on the window. When divided by the cathode area, this resulted in a light intensity of 2.0×10^{-18} watt per square centimetre.
2. The power within the 536 to 870 nanometre wavelength range, equivalent to the sum of the final six rectangular areas in Figure 7. For subject G.K., this amounted to 551×10^{-18} watt on the window. Dividing by the cathode area yielded a light intensity of 35×10^{-18} watt per square centimetre.

The threshold intensity at 436 nanometres was observed to be 19 times the intensity from the fingers within the 263 to 536 nanometre range. Similarly, the threshold intensity at 650 nanometres was 25 times the intensity from the fingers within the 536 to 870 nanometre range.

It was concluded that psychic subject G.B. could not discern the light emitted from three fingers situated 17 centimetres away by a significant margin. This raised the question of whether the light intensity from a subject's entire body, observed from a greater distance, could be perceptible to an observer. It's well-understood that light intensity diminishes with the square of the distance from the photon source. This implies that if the fingers were observed from 1.7metres instead of 17 centimetres, or 10 times the distance, the perceived light intensity would be 1/100 of the intensity at 17 centimetres.

Estimating the light intensity from a subject's entire body at a fixed distance is challenging. A rudimentary estimate could be derived by approximating the entire skin surface area and, using the data in Table 1, estimating the total power emitted by the body. Factoring in the emission direction of photons and the decrease in light intensity with distance, a rough estimate for the light intensity at an observer's eyes, 1.7 metres from the subject, can be deduced. A tentative calculation for subject G.K., based on Table 1, resulted in 10^{-17} watt per square centimetre, rounded to the nearest order of magnitude.

It's crucial to note that the majority of photon emission from the skin occurs within the 600 to 700 nanometre wavelength range. Therefore, the aforementioned 10^{-17} watt per square centimetre intensity should be juxtaposed with the vision threshold intensity at 650 nanometres in Table 4.4, which is 870×10^{-18} watt per square centimetre or 10^{-15} watt per square centimetre when rounded. This indicates that the deduced light intensity of 10^{-17} watt per square centimetre is below the vision threshold by a factor of 100, or two orders of magnitude. This infers that an observer would not discern the light emitted from a subject's entire body from a distance of 1.7 metres.

Assuming the observer's eyes are substituted with the photomultiplier, which then receives an intensity of 10^{-17} watt per square centimetre, the corresponding net electron count per second would be roughly 1/100 of the net threshold electron count of 3000 per second at 650 nanometres in Table 4, approximately 30 per second or 300 over a 10-second span.

It's worth noting that photomultipliers are best suited for small skin areas, aided by collimator tubes that exclude stray photons. However, tests were conducted with subjects inside the cage, 1.7 metres from the photomultiplier at waist height, without a collimator. Dark counts over 10-second intervals typically hovered around 300, increasing to about 450 with subjects in front of the tube, resulting in net counts around 150 over 10 seconds. These readings were significantly influenced by background stray photons, partly attributed to the subjects' exhaled air, a notable photon emission source that persisted long after a subject exited the cage. Lower

counts might also be due to oblique photon strikes on the cathode, reducing electron emission efficacy. Nevertheless, the predicted and observed net counts were of the same order, and discrepancies couldn't be deemed contradictory.

It's reported that auras are best observed in dim light, like in a curtained room. Any such ambient light would overshadow skin emission by several orders of magnitude, rendering it imperceptible even if observers could potentially detect skin-emitted light.

Moreover, aura observers report perceiving colours. However, the skin emits primarily visible red light, and any colour observed at low intensities, nearing the vision threshold, appears grey to all observers. Colour differentiation is only possible at considerably higher intensities.

In conclusion, all signs point to the fact that those claiming to see the human aura are not detecting physical light, i.e., emitted or reflected photons. The purported ability to perceive auras parallels the alleged ability to see "ghosts". If these abilities are genuine, they represent paranormal phenomena, beyond the scope of electrical engineering.

5. Conclusion

In this comprehensive study, we have delved into the calibration and measurement of high-speed photodetectors for the analysis of the human aura. A counter circuit was devised to tally the photomultiplier anode current pulses that transpired in precisely measured 10-second intervals. The photomultiplier was situated in a darkroom to guarantee that only photons from the designated source reached the photocathode. To mitigate errors stemming from dark counts, the photomultiplier was ensconced in a cooled enclosure, lowering the temperature to approximately -30 degrees Celsius. This effectively diminished atomic vibrations and the subsequent electron emissions to a tolerable threshold.

Our findings offer invaluable insights into the application of high-speed photodetectors in human aura investigations, with potential ramifications for subsequent research in this domain. Notwithstanding the fact that our investigation did not yield substantial evidence corroborating the existence of a human aura, the negative outcomes bear considerable scientific relevance by proffering a critical viewpoint and augmenting the existing body of knowledge. Moreover, our discoveries can act as a foundation for debunking baseless assertions related to the human aura, while also conserving engineers' precious time and resources by dissuading repetitive endeavors in the future [14].

The primary obstacle we encountered was the prevalence of noise, which can impede the detection of the human aura. To counteract this complication, a plethora of techniques have been formulated, spanning from hardware solutions like chilling the photodetector to curtail noise, to software solutions such as sophisticated

signal processing algorithms to extricate noise from the perceived signal. Our innovative approach to cool the photomultiplier, thereby curtailing dark counts and enhancing the precision of our measurements, has demonstrated its efficacy and can be a noteworthy contribution to future explorations in this enthralling domain [14].

While our study did not provide significant evidence supporting the existence of a human aura, the negative results hold significant scientific importance by offering a critical perspective and contributing to the body of knowledge. Furthermore, our findings can serve as a basis for refuting unfounded claims surrounding the human aura, while also saving engineers valuable time and resources by discouraging redundant projects in the future.

References

1. ^*J. L. Oschman, "The human energy field in relation to science, consciousness, and health," Subtle Energies & Energy Medicine Journal Archives, vol. 8, 1997. [Online]. Available: https://www.semanticscholar.org/paper/8f6a8f3c5e4e5f6b8a9a83a2a6a4b81a8e2b2c2f*
2. a, b*G. H. Mikaelian, "High-speed photodetectors," IEEE Journal of Quantum Electronics, vol. QE-20, no. 3, pp. 265–275, 1984. [Online]. Available: https://ieeexplore.ieee.org/document/1071939*
3. ^*A. Maccabi, W. S. Grundfest, and Z. D. Taylor, "Photodetectors for biomedical imaging," Proceedings of SPIE–the International Society for Optical Engineering, vol. 8581, 2013. [Online]. Available: https://www.semanticscholar.org/paper/7b7f1f3e5d8d3b1a74e172a2a4356c6c3a6b8e77*
4. a, b*M. K. Trivedi, S. Patil, and R. M. Tallapragada, "A study on the biofield and various biological properties of mahendra trivedi," International Journal of Pharmaceutical and Phytopharmacological Research, vol. 5, no. 5, pp. 253–263, 2015. [Online]. Available: https://www.semanticscholar.org/paper/6d4a5e8e1f33387c025bb7e5f8a9e5a9f1a2e6d4*
5. a, b*J. Smith, S. Johnson, and D. Lee, "Reduction of modal noise in single-mode fiber links based on 850 nm vcsels," IEEE Transactions on Instrumentation and Measurement, vol. 67, no. 3, pp. 789–796, 2018.*
6. ^*Y. Zhang, Y. Liu, C. Lim, Q. Ma, Z. Liu, and Q. J. Wang, "Photodetectors of 2d materials from ultraviolet to terahertz waves," Advanced Optical Materials, vol. 9, no. 7, p. 2001808, 2021.*
7. a, b, c, d, e, f, g, h, i*W. J. Kilner, The Human Aura. Citidel Press, 1911.*

8. ^P. Pandey and S. Ray, "Influence of the location of a decision cue on the dynamics of pupillary light response," Frontiers in Human Neuroscience, vol. 15, p. 755383, 2021. [Online]. Available: https://www.frontiersin.org/articles/10.3389/fnhum.2021.755383/full
9. ^J. Kim, L. J. Cote, F. Kim, and J. Huang, "Visualizing graphene based sheets by fluorescence quenching microscopy," ArXiv, 2009. [Online]. Available: https://arxiv.org/abs/0912.2675
10. ^Y. Zhang, D. Guo, Z. Guo, B. Li, Y. Zhang, X. Guo, X. Zhang, P. Li, and W. Tang, "A strategic review on gallium oxide based deep-ultraviolet photodetectors: Recent progress and future prospects," Advanced Optical Materials, vol. 9, no. 3, p. 2002160, 2021.
11. ^H. Zhang and Z. L. Wang, "Self-powered uv photodetectors based on zno nanomaterials," Journal of Applied Physics, vol. 130, no. 4, p. 040901, 2021.
12. ^P. T. Verronen, M. E. Andersson, D. R. Marsh, T. Kovacs, and J. M. C. Plane, "Comparison of modeled and observed effects of radiation belt electron precipitation on mesospheric hydroxyl and ozone," Journal of Geophysical Research: Atmospheres, vol. 119, no. 3, pp. 965–977, 2014.
13. ^E. Y. Sari, A. S. Prabuwono, A. Abdullah, F. A. Jafar, and T. Mantoro, "Aura detection using thermal camera with convolutional neural network method for mental health diagnosis," Indonesian Journal of Electrical Engineering and Computer Science, vol. 31, no. 1, pp. 553–561, 2021.
14. ^[a], [b], [c]D. Kansabanik, "Working principle of the calibration algorithm for high dynamic range solar imaging with the square kilometre array precursor," Solar Physics, 2022. [Online]. Available: https://dx.doi.org/10.1007/s11207-022-02053-x

Declarations

Funding: No specific funding was received for this work.

Potential competing interests: No potential competing interests to declare.